 doi:10.20944/preprints202208.0106.v1

Article

A *Dpagt1* Missense Variant Causes Early Degenerative Retinopathy without Myasthenic Syndrome in Mice

Lillian F. Hyde [1,†], Yang Kong [1,2,†], Lihong Zhao[1], Sriganesh Ramachandra Rao[3,4,5], Jieping Wang[1], Lisa Stone[1], Andrew Njaa[1], Gayle B. Collin[1], Mark P. Krebs[1], Bo Chang[1], Steven J. Fliesler[3,4,5], Patsy M. Nishina[1] and Jürgen K. Naggert[1*]

[1] The Jackson Laboratory, Bar Harbor, ME 04609
[2] The Graduate School of Biomedical Science and Engineering, University of Maine, Orono, ME 04469
[3] Departments of Ophthalmology and Biochemistry, Jacobs School of Medicine and Biomedical Sciences, The State University of New York, Buffalo, New York, USA
[4] Neuroscience Graduate Program, University of Buffalo, The State University of New York, Buffalo, New York, USA
[5] Research Service, VA Western New York Healthcare System, Buffalo, New York, USA
† These authors contributed equally to the work.
* Correspondence: juergen.naggert@jax.org; (207) 288-6064

Abstract: Congenital Disorders of Glycosylation (CDG) are a heterogenous group of primarily autosomal recessive mendelian diseases caused by disruptions in the synthesis of lipid linked oligosaccharides and their transfer to proteins. CDGs affect multiple organ systems and vary in presentation, even within families. Here we describe a chemically induced mouse mutant, *tvrm76*, with early onset photoreceptor degeneration. The recessive mutation was mapped to Chromosome 9 and associated with a missense mutation in the *Dpagt1* gene encoding UDP-N-acetyl-D-glucosamine:dolichyl-phosphate N-acetyl-D-glucosaminephosphotransferase (EC 2.7.8.15). The mutation is predicted to cause a substitution of aspartic acid with glycine at residue 166 of DPAGT1. Increased expression of *Ddit3*, and elevated levels of HSPA5 (BiP) suggest the presence of early-onset endoplasmic reticulum (ER) stress. These changes were associated with induction of photoreceptor apoptosis in *tvrm76* retinas. Mutations in human *DPAGT1* cause Myasthenic Syndrome 13 and severe forms of Congenital Disorder of Glycosylation Type Ij. In contrast, *Dpagt1*^{tvrm76} homozygous mice present with congenital photoreceptor degeneration without overt muscle or muscular junction involvement. Our results suggest the possibility of *DPAGT1* mutations in human patients that present primarily with retinitis pigmentosa with little or no muscle disease. Variants in DPAGT1 should be considered when evaluating cases of non-syndromic retinal degeneration.

Keywords: DPAGT1; Congenital Disorders of Glycosylation; sensitized chemical mutagenesis screen; mouse genetics; inherited retinal disease; ER Stress

1. Introduction

Congenital Disorders of Glycosylation (CDG) Type 1 are a family of autosomal recessive diseases caused by defects in the synthesis of dolichol lipid-linked oligosaccharides and their transfer to proteins in the endoplasmic reticulum (ER) [1-3]. Currently there are 28 genes known to cause the disease (OMIM PS212065) whose presentation is highly variable, even within families that carry the same mutation[3-5]. In this study, we primarily focus on the role of a dolichol phosphate N-acetylglucosamine-1-phosphotransferase (DPAGT1) variant in the pathological events leading to retinal degeneration, which has yet to be fully elucidated.

The *DPAGT1* gene encodes an integral ER membrane enzyme[1,6], which is ubiquitously expressed and catalyzes the first step of *N*-glycosylation, the predominant form of glycosylation in eukaryotes that governs protein folding and quality control [7]. Glycosylation is an essential process in growth and development, and the most common post-

 doi:10.20944/preprints202208.0106.v1

translational modification of lipids and proteins[8]. In human populations, *DPAGT1* missense mutations are associated with limb girdle congenital myasthenic syndrome 13 (CMS13; OMIM 614750) and congenital disorders of glycosylation type Ij (CDG1J; OMIM 608093), both characterized by defects in cognitive or motor abilities [9-11]. Retinal abnormalities, as a prominent pathological feature are occasionally noted in CDG patients [12,13]. DPAGT1 is the primary mechanistic target of tunicamycin, a pharmacological agent which triggers secondary ER stress and the unfolded protein response (UPR) by blocking DPAGT1-dependent protein glycosylation [7,14]. Intravitreal injection of tunicamycin causes retinal degeneration driven by opsin hypoglycosylation [15,16], yet DPAGT1 function in the neural retina has not been thoroughly investigated.

Perhaps not surprisingly, given the critical role of DPAGT1 in glycosylation, null mutations in *Dpagt1* lead to embryonic lethality in mice[17]. However, through the Translational Vision Research Models (TVRM) mutagenesis program[18,19], we identified a viable mouse line, *tvrm76*, which harbors a recessive D166G missense mutation in *Dpagt1*. The *tvrm76* mutants were initially identified by a grainy fundus appearance with an attenuation of retinal vessels by indirect ophthalmoscopy. This clinical phenotype was associated with an early-onset photoreceptor degeneration as assessed by histology. Biochemical characterization of the mutant revealed that increased ER stress may contribute to the cell death observed in the retina. Further study of the *tvrm76* mutant may provide additional insights into the role of glycosylation in retinal health and the mechanism through which *Dpagt1*^{tvrm76} mediates its effects on photoreceptor degeneration and will serve as a unique model for investigating retinopathies reported in CDG patients.

2. Results

2.1. Homozygosity of the Dpagt1^{tvrm76} allele causes early onset retinal degeneration

Through screening of N-ethyl-N-nitrosourea (ENU) mutagenized C57BL/6J mice by indirect ophthalmoscopy, a strain with pronounced degenerative fundus changes and progressive pigmentary retinopathy was observed and named *tvrm76*. In order to determine the molecular basis of the *tvrm76* variant, linkage analysis was performed. A recessive locus associated with the retinopathy was identified on Chromosome 9 within approximately a 20 cM region between markers *D9Mit129* and *D9Mit11*. Whole exome sequencing revealed a missense mutation in exon 3 of *Dpagt1,* in which adenine 497 is replaced by guanine (c.497A>G, Fig. 1A, B). The *Dpagt1* mutation co-segregated with a degenerative phenotype in backcross progeny from the mapping cross as determined by indirect ophthalmoscopy and by optical coherence tomography (OCT, Fig. 1E, F). The A>G nucleic acid transition is predicted to cause a substitution of an aspartic acid residue by glycine (D166G). By comparison with the 3D structure of human DPAGT1 (UniProt Q9H3H5), the mutated amino acid is located in an interfacial loop between transmembrane α-helical segments 4 and 5 of the DPAGT1 protein and is conserved among species (Fig. 1C, D). Measuring *Dpagt1* expression levels using qPCR showed a slight increase in expression in eyes of mice homozygous for the *tvrm76* mutation relative to wild type controls, however the difference between groups was not significant (Fig. 1L).

In addition to the morphological characterization of the degenerative change, we also assessed retinal function in *tvrm76* mice, using electroretinography (ERG) at one and three months of age. The scotopic a-wave and b-wave responses, associated primarily with rod photoreceptor function, were significantly impaired in one-month-old *tvrm76* homozygotes in comparison to the wild type littermates, and markedly deteriorated with age (Fig. 1G, I, J). Likewise, photopic b-waves were also significantly compromised in *tvrm76* homozygotes at three months of age (Fig. 1H, K). The functional losses were concomitant with the observed loss of photoreceptors.

Preprints (www.preprints.org) | NOT PEER-REVIEWED | Posted: 4 August 2022 doi:10.20944/preprints202208.0106.v1

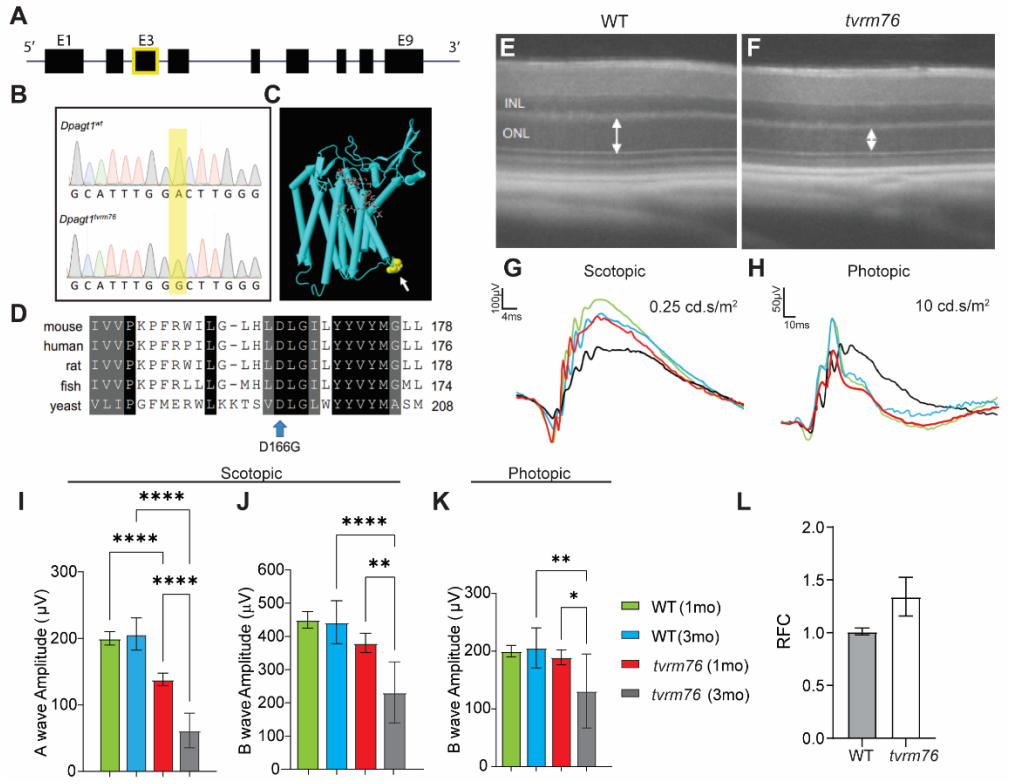

Figure 1. Identification of the *tvrm76* mutation and phenotypic characterization in the retina. **(A)** Genomic structure of *Dpagt1*. Whole exome sequencing revealed a missense mutation in exon 3 of *Dpagt1* (E3, boxed in yellow) **(B)** The mutation results in a transition of adenine to guanine (c.497A>G, shaded in yellow) resulting in an amino acid substitution (aspartic acid (D) to glycine (G)) at residue 166. **(C)** DPAGT1 protein structure. Yellow arrow indicates location of domain variant. **(D)** Alignment of DPAGT1 amino acid sequences from different species around the *tvrm76* variation. Blue arrow indicates location of D166G missense mutation. **(E,F)** A representative OCT image of a *tvrm76* mutant compared to a wildtype (WT) littermate control**.** Double arrows indicate thickness of outer nuclear layer (ONL)**.** INL, inner nuclear layer. **(G-K)** ERG recordings in *tvrm76* mutants at 1 and 3 months of age. **(G,I,J**) Average scotopic rod response (flash stimuli: 0.25 cd·s/m2). **(H,K)** Average photopic cone response (flash stimuli: 10 cd·s/m2). Results are mean ± SEM. n = 5-9 ****: p<0.0001;**p<0.01;*p<0.05 (Ordinary one-way ANOVA). **(L)** mRNA relative fold change (RFC) of *Dpagt1* by qRT-PCR analysis. Results are mean ± SEM. n = 5 (p = 0.0819, Student t-test).

Understanding the role of *Dpagt1 in vivo* is difficult because null mutants are embryonic lethal [17]. To better characterize the effects of the *Dpagt1*^{tvrm76} mutation, we created two additional models (Fig. 2A). The first, referred to as Rho iCre(+)-*Dpagt1*$^{flox/flox}$, harbors a tissue specific knockout allele of *Dpagt1* in rod photoreceptor cells, and was created by outcrossing a homozygous *Dpagt1* floxed model, B6.129-*Dpagt1*^{tm2Jxm}/J, with a transgenic mouse expressing rod photoreceptor specific Cre recombinase, B6.Cg-*Pde6b*$^{+}$ *Tg(Rho-icre)1Ck*/Boc [20] and subsequently backcrossing Rho iCre(+)-*Dpagt1*$^{flox/+}$ progeny to homozygous *Dpagt1* floxed mice. The second model, referred to as Rho iCre(+)-*Dpagt1*$^{flox/tvrm76}$, bears one conditional null allele of *Dpagt1* and one *Dpagt1*^{tvrm76} allele.

To assess the phenotypic changes associated with the *tvrm76* mutation, we performed fundoscopic examinations of *tvrm76* homozygotes at one and three months of age. Fundus images of mutant mice showed a progressively grainy appearance, consistent with photoreceptor degeneration[21,22] (Fig. 2B-C). Rho iCre(+)-*Dpagt1*$^{flox/tvrm76}$ compound heterozygotes (Fig. 2E-F) and Rho iCre(+)-*Dpagt1*$^{flox/flox}$ homozygotes (Fig. 2H-I) displayed a more severe graininess, suggesting advanced degeneration by 3 months of age compared to *Dpagt1*^{tvrm76} homozygotes. This was consistent with our expectations that *Dpagt1* is necessary for proper photoreceptor cell viability and function.

Preprints (www.preprints.org) | NOT PEER-REVIEWED | Posted: 4 August 2022 doi:10.20944/preprints202208.0106.v1

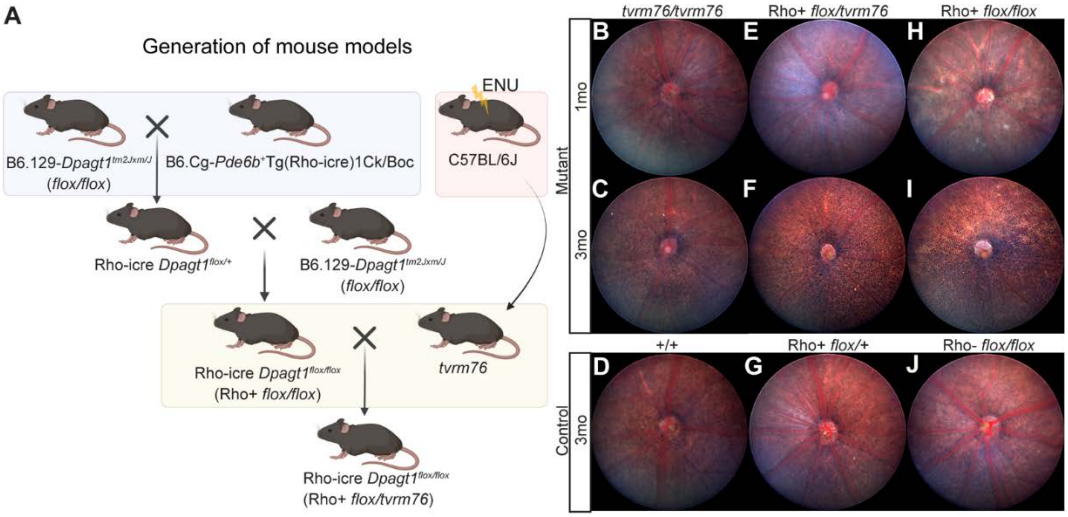

Figure 2. Generation and phenotypic characterization of *tvrm76* and a rod photoreceptor-specific D*pagt1* conditional knockout by fundoscopy. **(A)** Breeding schematic for *tvrm76* and *Dpagt1* conditional knockout models. *tvrm76*, a recessive RP model, was identified through a phenotypic-driven screen of putative mutants (putants) generated by chemical mutagenesis (ENU) of C57BL/6J mice and subsequent intercrossing. For localized disruption of *Dpagt1* in photoreceptors, $Dpagt1^{tm2Jxm}$ was bred to a transgenic mouse expressing rhodopsin-iCre. Subsequently Rho icre (+) $Dpagt1^{flox/+}$ heterozygous progeny were backcrossed to homozygous *Dpagt1-* floxed mice to generate Rho iCre(+)-$Dpagt1^{flox/flox}$ mice (Rho+ *flox/flox*). For allelic testing, Rho iCre(+)- $Dpagt1^{flox/flox}$ mice were crossed to a $Dpagt1^{tvrm76}$ heterozygote to produce Rho iCre(+)-$Dpagt1^{flox/tvrm76}$(Rho+ *flox/tvrm76*) compound heterozygotes. **(B-J)** Representative funduscopic images of central retina in mutant strains and controls at 1 and 3 months of age. **(B-C)** $Dpagt1^{tvrm76}$ homozygotes, **(D)** wild-type (+/+) littermates. **(E-F)** Compound heterozygous (Rho+ *flox/tvrm76*), **(H-I)** Rho+ *Dpagt1*-floxed homozygotes and **(G)** Rho+ *flox/+* and **(J)** Rho- *flox/flox* controls.

To confirm the causal relationship of the $Dpagt1^{tvrm76}$ allele and the degenerative phenotype observed by fundoscopy, we examined retinal histological sections from $Dpagt1^{tvrm76}$ homozygotes, Rho iCre(+)-$Dpagt1^{flox/tvrm76}$ compound heterozygotes, Rho iCre(+)-$Dpagt1^{flox/flox}$ homozygotes, and littermate wildtype controls at postnatal day 14, one month, and three months of age (Fig. 3A). At three months of age, the compound heterozygotes developed pronounced photoreceptor degeneration, thus confirming that the mutation in $Dpagt1^{tvrm76}$ leads to retinal degeneration in mice. Photoreceptor degeneration was assessed using the ratio of nuclei from the outer nuclear layer (ONL) to the inner nuclear layer (INL). Measurements were made at three distances from the optic nerve head central (500 µm, Supplementary Fig.1A), mid-peripheral (1000 µm, Fig. 3B), and peripheral (1500 µm, Supplementary Fig.1A) to confirm the effects were consistent across the retina. In mid-peripheral sections (Fig. 3), no differences in the ONL/INL ratio were observed among mutants and their wildtype controls at 14 days of age. At one month, only homozygous $Dpagt1^{tvrm76}$ mutants showed significant degeneration in contrast to the Rho iCre(+)-$Dpagt1^{flox/tvrm76}$ compound heterozygotes and Rho iCre(+)-$Dpagt1^{flox/flox}$ homozygotes, which were similar to wildtype littermates. At one month, the peripheral retina appeared similar among all models (Supplementary Fig. 1A). Interestingly, by three months, the compound heterozygotes and homozygous Rho iCre(+)-$Dpagt1^{flox/flox}$ mutants surpassed $Dpagt1^{tvrm76}$ homozygotes in their degree of photoreceptor degeneration, with the homozygous Rho iCre(+)-$Dpagt1^{flox/flox}$ mutant having complete ONL loss (Fig. 3B). Interestingly, compound heterozygotes showed a significant thinning of photoreceptors, intermediate between the $Dpagt1^{tvrm76}$ and Rho iCre(+)-$Dpagt1^{flox/flox}$ homozygotes in severity. The total loss of photoreceptors observed in the homozygous Rho iCre(+)-$Dpagt1^{flox/flox}$ model indicates that DPAGT1 is essential for ONL maintenance, and the slower rate of

Preprints (www.preprints.org) | NOT PEER-REVIEWED | Posted: 4 August 2022 doi:10.20944/preprints202208.0106.v1

degeneration in *tvrm76* indicates that the *tvrm76*-associated D166G mutation is hypomorphic and is likely to retain some function.

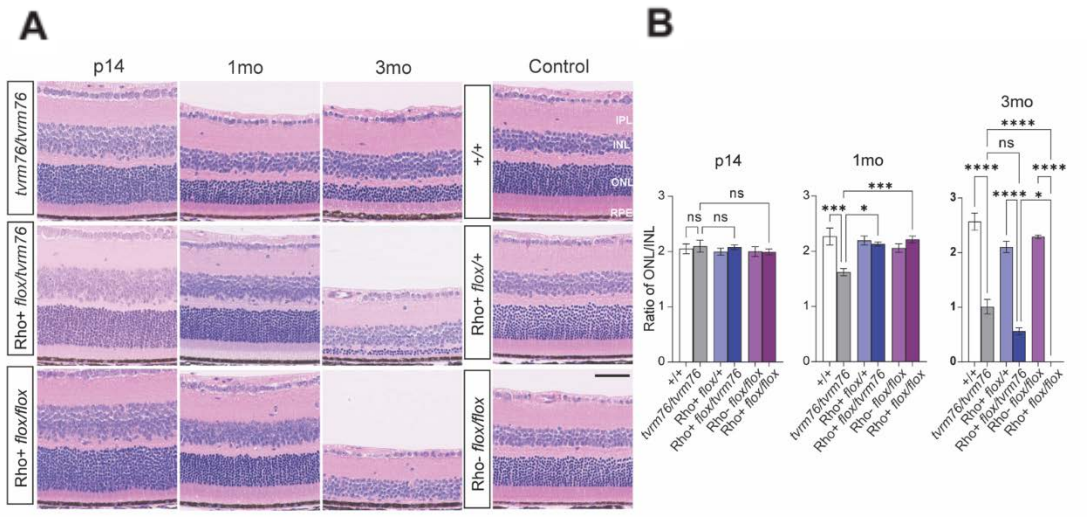

Figure 3. Histological analysis of homozygous *Dpagt1*^{tvrm76} and homozygous Rho iCre(+)-*Dpagt1*$^{flox/flox}$ models shows progressive photoreceptor degeneration in the mid-periphery of the retina. **(A)** Hematoxylin and eosin (H&E) staining of posterior eye sections from *Dpagt1*^{tvrm76} homozygotes, compound heterozygotes (Rho+ *flox/tvrm76*) and homozygous Rho iCre(+)-*Dpagt1*$^{flox/flox}$ (Rho+ *flox/flox*) models at postnatal day 14 (p14), one month (1mo), and three months (3mo) and three month littermate controls. **(B)** Quantification of ONL nuclei degeneration relative to INL. Scale bar = 50μm. Values represent mean ±SEM; n=3-6. *p<0.05; ***p<0.001; ****p<0.0001 (one-way ANOVA). IPL: inner plexiform layer; INL: inner nuclear layer; OPL: outer plexiform layer; ONL: outer nuclear layer; RPE: retinal pigment epithelium.

2.2. The Dpagt1^{tvrm76} *variant is not associated with aberrant protein glycosylation at an early age.*

DPAGT1 carries out the glycan tree transfer (oligosaccharyl transferase activity) in *N*-linked glycosylation of proteins. Because many retinal proteins are normally glycosylated, their aberrant glycosylation might contribute to the degenerative retinopathy in *Dpagt1*^{tvrm76} homozygotes. However, qualitative examination of global glycosylation of retinal proteins by western blot analysis at two and four weeks of age failed to show differences in glycosylation between homozygous *Dpagt1*^{tvrm76} and wild-type mice (Fig. 4A, B).

Specific retinal proteins that undergo *N*-glycosylation include opsin. Opsin glycosylation defects lead to autosomal dominant retinitis pigmentosa[23-25]. Since it is conceivable that aberrant opsin glycosylation might contribute to the degenerative retinopathy in homozygous *Dpagt1*^{tvrm76} mice, we tested the *N*-glycosylation status of opsin. The glycosylation pattern of rhodopsin did not differ between mutants and wild-type at two weeks of age (Fig. 4C). To increase the sensitivity to detect hypomorphic effects of the *Dpagt1*^{tvrm76} allele on *N*-linked glycosylation of rhodopsin, rhodopsin glycosylation was measured at two weeks of age in compound heterozygous (Rho iCre(+)-*Dpagt1*$^{flox/tvrm76}$) mutants. Retinas from Tg(RHO*T17M)5Asl mice[26] served as a positive control, wherein opsin exhibited an electrophoretic mobility shift of ~1 kDa. Additionally, PNGase-F treated wild-type retinal protein lysate (to enzymatically deglycosylate proteins including opsin) served as a true positive control, wherein opsin exhibits a mobility shift of about 2 kDa, in agreement with previous findings[24]. Again, no difference was noted compared to homozygous *Dpagt1*^{tvrm76} and wild-type controls (Fig. 4C).

Preprints (www.preprints.org) | NOT PEER-REVIEWED | Posted: 4 August 2022 doi:10.20944/preprints202208.0106.v1

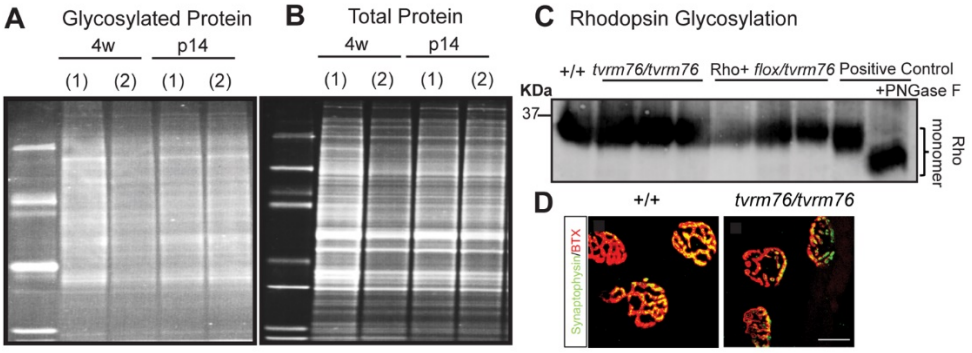

Figure 4. Protein glycosylation analysis in *Dpagt1*^{tvrm76} homozygotes. **(A-B)** No difference detected in glycosylated or total protein levels observed by SDS-PAGE analyses in *Dpagt1*^{tvrm76} homozygotes (2) and their wild-type (+/+) littermates (1) at four and two weeks of age. **(C)** Western blot of rhodopsin from *Dpagt1*^{tvrm76} homozygotes and compound heterozygotes (Rho+ *flox*/*tvrm76*) shows no glycosylation defect compared to defect model and positive PNGase control at two weeks of age (n=3). **(D)** Immunostaining of muscle tissue whole mount (tibialis anterior) dissected from homozygous *Dpagt1*^{tvrm76} vs +/+ against α-synaptophysin (green) and α-Bungarotoxin (BTX, green). Scale bar = 5μm.

2.3. Homozygous Dpagt1^{tvrm76} *mice do not recapitulate early muscular abnormalities observed in patients with DPAGT1 mutations.*

Since *DPAGT1* mutations are linked to congenital muscle weakness conditions in the human population, it prompted us to test whether *Dpagt1*^{tvrm76} homozygotes had muscle defects at a young age as well. A grip strength survey revealed similar grip strength between *Dpagt1*^{tvrm76} homozygotes and their wild-type littermates at one month of age (Supplementary Fig. 2A). Neuromuscular junctions in *Dpagt1*^{tvrm76} muscle tissue were also examined. Muscle whole mounts from *Dpagt1*^{tvrm76} mutants and controls were stained with anti-synaptophysin, which labels pre-synaptic vesicles, and with α-bungarotoxin (BTX) which binds the acetylcholine receptor (AchR) and localizes to the post-synapse of neuromuscular junctions. Our data showed a similar structural pattern of neuromuscular junctions in *Dpagt1*^{tvrm76} homozygotes and wild type controls (Fig. 4D). Transmission electron microscopy of muscle did not show the tubular aggregates that are often seen in human patients with CMS [9] (Supplementary Fig. 2B-E). Within the detection capacity of our assays, homozygous *Dpagt1*^{tvrm76} mice at a young age do not appear to recapitulate the early-onset myasthenic conditions associated with aberrant glycosylation in human patients.

2.4. Homozygous Dpagt1^{tvrm76} *eyes show signs of ER stress*

Since our results did not indicate significant defects in protein post-translational modification associated with the *Dpagt1*^{tvrm76} variant, we hypothesized activation of endoplasmic reticulum stress could mediate the mutation's pathogenic effects. Defective glycosylation disrupts normal post-translational modification of proteins and their proper maturation [27]. This disruption can affect the release of the abnormal proteins from the ER and lead to excessive protein accumulation and ER stress [28]. ER stress in turn can induce cell death [29-31]. To test if the mechanism underlying the photoreceptor degeneration in *Dpagt1*^{tvrm76} eyes might be attributable to a disturbance of ER homeostasis, a panel of ER-stress-associated molecules, including *Hsp90b1* (*Grp94*), *Hspa5* (*Bip*), *Ddit3* (*Chop*), *Atf4*, and *Padi2* (*Pdi*) were measured at the transcript level by qRT-PCR at two weeks of age, prior to the onset of photoreceptor degeneration (Fig. 5A). Notably, *Ddit3* was significantly upregulated in whole eyes of two-week-old animals. *Hsp90b1*, *Hspa5* and *Atf4* also showed increased expression relative to wild-type littermate controls.

To localize ER stress within the retinal layers, immunofluorescent staining of HSPA5 (BiP) was done. Increased staining was observed in the inner nuclear layer (INL), retinal

Preprints (www.preprints.org) | NOT PEER-REVIEWED | Posted: 4 August 2022 doi:10.20944/preprints202208.0106.v1

ganglion cell layer (RGC), and photoreceptor inner segments of *Dpagt1*^{tvrm76} homozygotes compared to wild-type littermate controls (Fig. 5B). The ER of photoreceptors is known to be localized in the inner segments, coinciding with our prediction of ER stress. Collectively, our observations revealed elevated levels of key ER-stress molecules in *tvrm76* mutant eyes, indicative of perturbances in ER homeostasis.

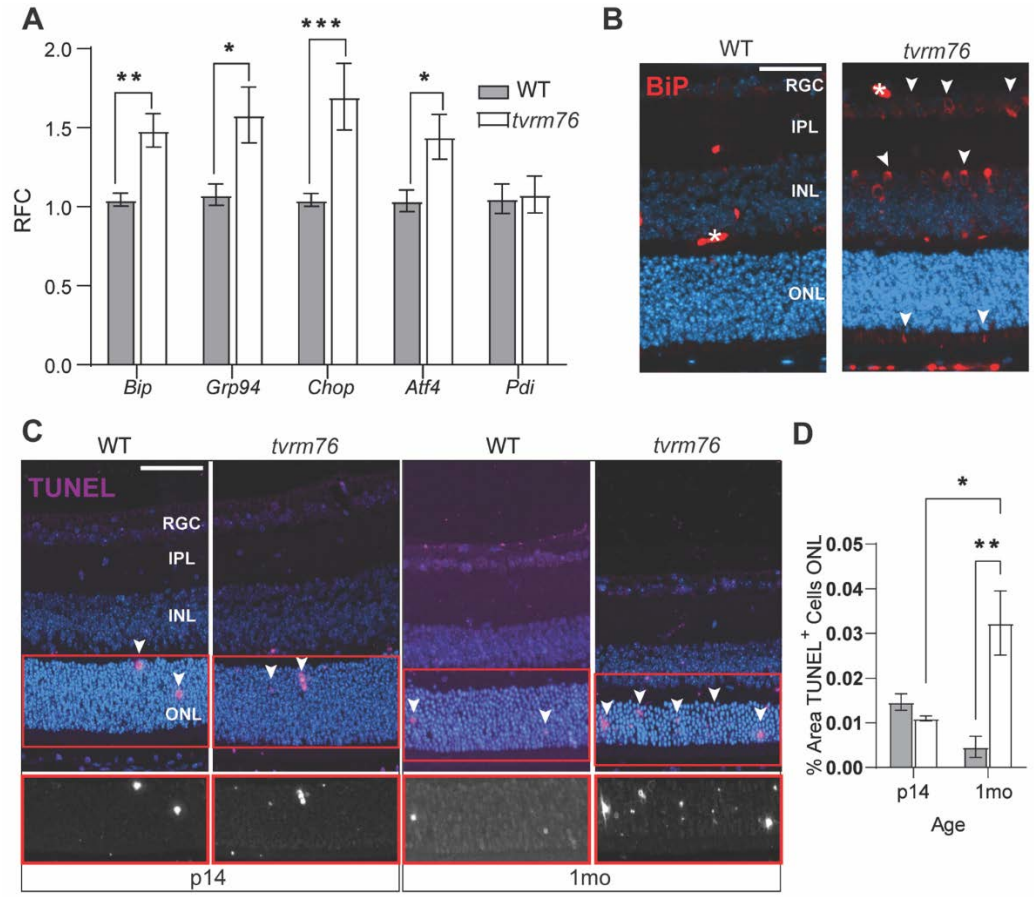

Figure 5. Degenerative retinopathy as a possible consequence of ER-mediated stress response**. (A)** q-RTPCR analysis of ER stress-associated markers in homozygous *Dpagt1*^{tvrm76} vs wildtype. Values show mean ± SEM (n=5). Student t-test; *p<0.05; **p<0.01; ***p<0.001. **(B)** Immunostaining of HSPA5 (BiP) (red) in *Dpagt1*^{tvrm76} homozygote vs wildtype shows increased staining in the inner segments, INL, and RGC layers (white arrowheads). Blood vessel (white *). **(C)** TUNEL staining (purple) of cell apoptosis in the retina at fourteen days (p14) and one month (1mo) of age in *Dpagt1*^{tvrm76} homozygotes compared with wildtype. Arrows point to apoptotic cells. Boxed area in lower panel shows TUNEL staining (white) without DAPI. Scale bar (B,C) = 50µm **(D)** Quantification of TUNEL+ cells in ONL show increase at one month in *Dpagt1*^{tvrm76} homozygotes. (n=3). One-way ANOVA * $p < 0.05$, ** $p < 0.01$. RGC: retinal ganglion cell layer; IPL: inner plexiform layer; INL: inner nuclear layer; OPL: outer plexiform layer; ONL: outer nuclear layer; RPE: retinal pigment epithelium. .

2.5. Increased number of apoptotic cells are detected in Dpagt1^{tvrm76} *retinas.*

We next sought to determine the pathological consequences that might arise from ER stress. Considering the significant loss of photoreceptors in homozygous *Dpagt1*^{tvrm76} retinas, we examined whether cell-induced apoptosis was detectable by TUNEL assay. A greater number of apoptotic cells were present in *Dpagt1*^{tvrm76} retinas compared to their wild-type counterparts at one month of age, which may underlie the observed loss of retinal cells (Fig. 5C-D). The observed increased TUNEL staining supports initiation of cell apoptosis perhaps due to elevated ER stress and substantiates retinal degeneration starting at a young age in *Dpagt1*^{tvrm76} homozygotes.

 doi:10.20944/preprints202208.0106.v1

3. Discussion

The *tvrm76* mutant was identified in an ENU mutagenesis screen, as a strain carrying a recessive mutation causing early-onset retinal degeneration. A missense mutation in *Dpagt1* which is predicted to change aspartate 166 to glycine (D166G), was identified and its causative role in photoreceptor cell loss was confirmed by observing retinal degeneration in compound heterozygous, Rho+ *Dpagt1*$^{flox/tvrm76}$, animals. The D166G mutation lies within the luminal loop between transmembrane segments 4 and 5, which contain residues, predicted to interact with the dolichol-phosphate binding site. Furthermore, two severe CDGIj mutations in humans, L168P and Y170C, are localized in close proximity to D166G and retain only 25% of wild type enzymatic activity [11]. Mutations occurring in these regions significantly diminish catalytic activity of the molecule whereas those that are distant from the active sites result in a smaller change in enzymatic activity [7,9,11,32,33]. However, in a qualitative assessment of glycosylation in homozygous *Dpagt1*^{tvrm76} eyes, we saw no noticeable difference in global and rhodopsin glycosylation at four and two weeks of age, respectively. This suggests that *Dpagt1*^{tvrm76} is a hypomorphic allele with sufficient activity to maintain near normal glycosylation levels in the retina.

Dpagt1^{tvrm76} mutant mice may serve as a novel model for studying degenerative retinopathy due to defects associated with reduced DPAGT1 function. In clinics, many patients bearing mutations in *DPAGT1* manifest multiple neurological symptoms [34-37]. Previous studies have primarily focused on the muscular presentations while eye symptoms are rarely addressed [38-41]. In this study, we found that the *Dpagt1*^{tvrm76} model recapitulates the retinal degeneration found in some human patients and enables researchers to better probe the pathogenesis of degenerative changes in retina caused by *DPAGT1* mutations. *Dpagt1* knockout mice are embryonic lethal [17,42] precluding the study of DPAGT1 in the retina. Therefore, the rod photoreceptor-specific B6.129-*Dpagt1*^{tm2Jxm}/J model provides a unique opportunity to study DPAGT1 function in this cell type. Future investigations using the rod photoreceptor-specific *Dpagt1* deletion will facilitate the understanding of DPAGT1-dependent protein glycosylation in retinal development and/or maintenance.

Typically, patients harboring *DPAGT1* variants present with limb-girdle weakness [43,44] and retinal degeneration is not noted. In this study, overt myasthenic manifestations were not detected in *Dpagt1*^{tvrm76} homozygotes. This is unlikely to be due to a specific affected isoform of DPAGT1, since all annotated splice variants carry the 166G mutant allele. While we only examined the grip strength of *Dpagt1*^{tvrm76} homozygotes at one-month of age, at six-months of age, the animals also did not show any apparent muscular weakness compared to the wild type during normal ambulation. Additional examination at an advanced age would be desirable to assess potential long-term effects of the *Dpagt1*^{tvrm76} mutation on muscle function. It should be noted that a large number of patients harboring *DPAGT1* variants were subject to underdiagnosis in clinics as well [36,43-45]. Nevertheless, our results demonstrate that *Dpagt1* mutations exist that primarily present with an eye phenotype with minimal muscle involvement. It is possible that the observed phenotype depends on a combination of a specific allele and genetic background modifiers, especially since variation in disease severity has been observed in human patients [41,43,46].

Proper glycosylation of a large array of proteins is important for their correct folding and stability [47-50]. Since glycosylation primarily occurs in the ER, accumulation of misfolded proteins there can result in ER stress and induction of the unfolded protein response (UPR) [51-53]. Assessment of ER stress and UPR in human CDG has been carried out using patient-derived fibroblasts [11] and genetically engineered cell lines[54]. These experiments did not show an activation of UPR in fibroblasts carrying *DPAGT1* mutations. However, the mutant cells were more sensitive to the ER stressor tunicamycin than control cells [11]. Concordantly, we observed only a moderate 30-70% increase in the expression levels of ER stress markers and a presence of HSPA5 (BiP) positive cells in the

 doi:10.20944/preprints202208.0106.v1

eyes of homozygous *Dpagt1*^{tvrm76} mice. Whether this modest increase in ER stress, unfolded protein response, and DDIT3 (CHOP) activation is solely responsible for the observed apoptosis of photoreceptor cells in our model is currently unconfirmed.

The results presented here demonstrate that *DPAGT1* mutations may exist that predominantly present at an early age as a non-syndromic retinal degeneration. *DPAGT1* should, therefore, be considered as a candidate gene for retinal diseases that map within its vicinity. The *Dpagt1*^{tvrm76} model may be useful for pathological studies to better understand how a mutation in *Dpagt1* leads to a retinal degenerative phenotype. In addition, the viability of *Dpagt1*^{tvrm76} makes it an attractive model for studying the role of DPAGT1 in other organ systems not examined in this study.

4. Materials and Methods

4.1. Mice, Mutagenesis, and Husbandry

All of the mice involved in this study were bred and housed in the Research Animal Facility at the Jackson Laboratory, and study protocols used in this project were reviewed and approved by the JAX Institutional Animal Care and Use Committee. Male C57BL/6J (B6/J, 000664) were mutagenized (G_0) at 10-12 weeks of age by weekly intraperitoneal injections of N-ethylnitrosourea (Sigma, Cat #N3385) of 70 mg/kg body weight for three consecutive weeks. The G_0 mice were mated with un-mutagenized female B6/J to produce G_1 progeny, which were subsequently mated to female B6/J to produce a G_2 population. G_2 females were backcrossed to their G_1 sires to produce G_3 mice, which were screened at 12 weeks for ocular phenotypes by indirect ophthalmoscopy. A G_3 male mouse was found to have a fundus with grainy appearance. Because the G_3 mouse did not breed, G_3 siblings were intercrossed to confirm heritability and establish the line, named *tvrm76* (C57BL/6J-*Dpagt1*^{tvrm76}/Pjn), which was inherited in a recessive manner. From these initial matings, we determined that both homozygous *tvrm76* male and female mice did not breed.

To conditionally knockout *Dpagt1* in rod photoreceptors, mice bearing a *Dpagt1* floxed allele, B6.129-*Dpagt1*^{tm2Jxm}/J (JAX:006887), were crossed to B6.Cg-*Pde6b*$^{+}$ Tg(Rho-icre)1Ck/Boc (JAX:015850) and backcrossed to generate mice homozygous for the floxed *Dpagt1* allele and carrying the rod-expressing Rho-icre transgene (Rho iCre(+)-*Dpagt1*$^{flox/flox}$).

4.2. Identification of the molecular basis of tvrm76

Due to infertility of homozygous *tvrm76* mutants, progeny-tested heterozygous mice were used in mapping experiments. C57BL/6J-*Dpagt1*^{tvrm76}/Pjn heterozygotes were outcrossed to strain DBA/2J and resulting F1s were either backcrossed to C57BL/6J-*Dpagt1*^{tvrm76}/Pjn heterozygotes or B6:D2-*Dpagt1*^{tvrm76} heterozygotes. In the former instance, only affected mice (grainy fundus) were used for linkage analysis. The chromosomal location of the *tvrm76* locus was identified by genotyping 48 MIT markers across the genome in 24 affected mice from the linkage crosses. To identify the causative mutation, high-quality genomic DNA was prepared from *tvrm76* homozygotes for preparation of exome capture libraries which were sequenced with on a HiSeq 2000 sequencing system (Illumina) as previously described[55]. Whole-exome sequencing of *tvrm76* identified a missense mutation in *Dpagt1*, which was subsequently confirmed by Sanger sequencing.

4.3. Phenotyping

The fundus of mouse eyes was examined using a Heine Omega 500 indirect ophthalmoscope with a 60-diopter aspheric lens[56]. Fundus images were captured using a Micron IV camera (Phoenix Research Laboratories) after topical administration of 1% atropine sulphate for pupil dilation, and Goniovisc hypromellose ophthalmic solution for surface lubrication and formation of a fluid bridge, as necessary[57]. Non-invasive sectional examination of mouse retinas was performed using a Bioptigen ultra-high resolution (UHR) Envisu R2210 spectral domain OCT (SDOCT)[57]. Mice eyes were dilated using 1%

 doi:10.20944/preprints202208.0106.v1

cyclopentolate or 1% atropine and anesthetized with ketamine/xylazine (100 mg/mL ketamine, 20 mg/mL xylazine, and 0.9% w/v sodium chloride). The function of the outer retina was assessed by electroretinography (ERG). *Dpagt1*^{tvrm76} homozygotes and their wild type counterparts were examined at 1 and 3 months of age. ERG was recorded and analyzed following the routine protocol described previously [58]. The measure of mouse grip strength was determined by recording the duration of time a mouse held onto an inverted wire mesh screen. The experiment followed a previously published protocol[31]. In brief, *Dpagt1*^{tvrm76} homozygotes and their wild-type control mice were placed in the center of a wire mesh screen, which was subsequently inverted (T_0). The time when the mouse fell off was recorded (T_f).

4.4. Histology

For gross histology, eyes were enucleated from *Dpagt1*^{tvrm76} homozygotes and their sibling wild-type controls immediately after carbon dioxide asphyxiation. Tissues were fixed in acetic acid: methanol: phosphate buffer (1:3:4) prior to paraffin embedding and sectioning at 5 microns. Tissue sections were de-paraffinized and stained with hematoxylin and eosin (H&E) as previously described [58] and examined by light microscopy. Images were captured using a NanoZoomer 2.0-HT digital slide scanner (Hammamatsu) at 40x magnification.

4.5. Electron Microscopy

Gastrocnemius muscle was fixed in a mixture of glutaraldehyde (2.5%) and paraformaldehyde (2%) in sodium phosphate buffer. The samples were then post-fixed in 1% OsO_4 and rinsed in cacodylate buffer. After dehydration, tissue was embedded in Epon and sectioned for TEM cross-sectionally and longitudinally. Ultrastructure was imaged using a transmission electron microscope (Hitachi HT-7700).

4.6. RNA Extraction and Analysis

RNA was extracted from whole eyes of two-week old *Dpagt1*^{tvrm76} and wildtype littermates using TRIzol (Invitrogen, Cat #15596026) and the gentleMACS tissue dissociator (Miltenyi Biotec, Cat #130-093-235). The mRNA was extracted using RNeasy Mini Kit (Qiagen, Cat # 74104) following the protocol provided by the manufacturer. cDNA was synthesized using the SuperScript cDNA synthesis system (Invitrogen, Cat #18091200) and q-RTPCR was performed using iTaq Universal SYBR Green Supermix in the CFX96 Touch Real-Time PCR Detection System (Bio-Rad, Cat #1725121). The relative fold change was determined using the comparative CT method ($\Delta\Delta C_t$) and normalized to the level of β-actin (*Actb*) mRNA, an internal control calibrator. The primers are presented in Supplement Table 1.

4.7. Immunofluorescence

Enucleated eyes from two-week- and one-month-old *Dpagt1*^{tvrm76} mutants and wildtype littermates were fixed overnight in methanol:acetic acid in phosphate-buffered saline (PBS) at a ratio of 3:1:4. Tissues were subsequently embedded and sectioned at four μm for immunohistochemistry. Slides underwent a standard deparaffination and rehydration protocol. Antigen-retrieval was performed using 10 mM citrate buffer in a water bath set at 100℃ for 30 minutes. Nonspecific binding sites were blocked using 1:50 normal donkey serum and 0.5% Triton-X in PBS. Antibody incubation was performed as previously described [58]. To prepare muscle specimens for whole mount staining, tibialis anterior tissue was dissected and flattened immediately before overnight fixation with 4% paraformaldehyde (PFA) in PBS at 4℃. The muscle tissues were co-immunostained and mounted for imaging according to recommended procedures [59,60]. For detecting apoptotic cells, TUNEL assays were carried out by using the In Situ Apoptosis Detection, Alexa Fluor 647 Dye (Invitrogen, Cat #C10619) following the manufacturer's protocol. Samples

 doi:10.20944/preprints202208.0106.v1

were mounted in Vectashield (Vector Laboratories) and imaged using a Zeiss Axio Observer.z1 fluorescence microscope (Carl Zeiss Microscopy). The resulting images were processed in Fiji [61] using the Stack Focuser Macro. The ONL region was selected using a drawn boundary based on DAPI staining of photoreceptor cells and a threshold was set to measure the percent area of TUNEL-positive cells.

4.8. Antibodies

Antibodies used for immunofluorescence staining includes rabbit anti-GRP78 (1:200, Cell Signaling, Cat #C50B12), fluorophore 594-conjugated α-Bungarotoxin (1:1000, ThermoFisher Scientific, Cat #B13423) and rabbit anti-synaptophysin (1:200, Abcam, Cat #ab32127).

4.9. Western blot

To assess global protein glycosylation, the Pro Q Emerald 488 Glycoprotein Stain Kit (ThermoFisher Scientific, Cat #P21875) was used to stain SDS-PAGE gels with Sypro Ruby based on the manufacturer's protocol. Immunoblot analysis for opsin glycosylation was carried out as described elsewhere [62]. Briefly, retinas from C57BL6/J, *tvrm76* and Rho iCre(+)-*Dpagt1*$^{flox/tvrm76}$ mice were harvested and flash frozen immediately. Retinas were lysed in RIPA buffer (ThermoFisher Scientific, Cat #89900) supplemented with protease inhibitor cocktail (ThermoFisher Scientific, 78441) at 1:100 dilution. Protein content in the lysates was estimated using a Pierce™ BCA Protein Assay Kit (ThermoFisher Scientific, Cat #23225). Similarly processed RhoT17M/+ retina served as a positive control for opsin hypoglycosylation[63] (Tissues were a kind gift of Dr. Marina Gorbatyuk, UAB, Birmingham, USA). PNGase-F N-glycosidase assay (New England Biolabs Inc., Ipswich, MA, USA; Cat #P0704S) was carried out as per the manufacturer's instructions. About 20µg of C57BL6/J retinal protein lysate was treated with 200 U of PNGase-F in 1X Glycobuffer 2 (10X buffer provided with the kit) supplemented with 1% NP-40 detergent at 37℃, overnight. Protein lysates were subjected to Western blot analysis utilizing the following antibody mouse anti-opsin monoclonal antibody (Abcam, Burlingame, CA, USA; Cat #ab5417, 1:2000). Blots were then probed with appropriate host-specific alkaline phosphatase-tagged secondary antibodies (1h at room temperature). Detection of antibody binding was achieved using chemifluorescent enzyme substrate (GE Healthcare Life Sciences, Marlborough, MA, USA; Cat #45000947) and a ChemiDoc™ MP Imaging System (Bio-Rad Laboratories).

4.10. Image Analysis and Statistics

Fiji software [61] was used for image processing and western blot quantification. Statistical significance was analyzed by two-way ANOVA with post-hoc Bonferroni's multiple comparisons test, or student-*t* test for comparisons of two groups using GraphPad Prism version 8 (GraphPad Software, San Diego, CA, USA). At least three biological replicates were utilized in each group for statistical analysis. Results are shown as mean ± SEM., $p<0.05$ was reported as statistically significant.

Supplementary Materials:

Author Contributions: Conceptualization, P.M.N., J.K.N.; methodology, L.H.Z., S.R.R., M.P.K., S.J.F.; investigation, L.F.H., Y.K., G.B.C., L.H.Z., S.R.R., J.W., L.S., A.N. M.P.K.; resources, L.S., B.C.; writing—original draft preparation, L.F.H, Y.K., L.H.Z,.; writing—review and editing, L.F.H., Y.K., L.H.Z., S.R.R., A.N., G.B.C, M.P.K., B.C., S.J.F., P.M.N., J.K.N..; visualization, L.F.H.; supervision, S.J.F., P.M.N., J.K.N.; funding acquisition, S.R.R., M.P.K., B.C., S.J.F., P.M.N., J.K.N. All authors have read and agreed to the published version of the manuscript.

Funding: Research in this publication was supported by the National Eye Institute of the National Institutes of Health under award numbers R01EY011996 to P.M.N., R01EY027305 to P. M. N. and M.P.K., R01EY019943 to B.C., and R01EY028561 to J.K.N., and by The Jackson Laboratory, Director's Innovation Fund (DIF), award number 19000-13-12. SRR is the recipient of a Career Starter Research

 doi:10.20944/preprints202208.0106.v1

Grant Award from the Knights Templar Eye Foundation, Inc. SJF is the recipient of a Research Career Scientist Award (RCSA; I K6 BX005787) from the Department of Veterans Affairs, BLR&D Service. Supported, in part, by facilities and resources provided by the VA Western NY Healthcare System (SJF, SRR). The authors also wish to acknowledge the support of the JAX *Genome Technologies*, *Histopathology*, *and Microscopy Service*, supported in part by the National Cancer Institute of the National Institutes of Health under award number P30CA034196.

Institutional Review Board Statement: The animal study protocol was approved by the JAX Institutional Animal Care and Use Committee (protocol ACUC 99089, last approved 22 August 2020).

Data Availability Statement: Relevant data are contained within the article or supplementary material. Additional datasets generated and/or analyzed for the current study are available from the corresponding author.

Acknowledgments: We thank Wanda Hicks for assistance in phenotyping of mice. Illustrations were created with BioRender.com.

Conflicts of Interest: The authors declare no conflicts of interest.

Appendix A

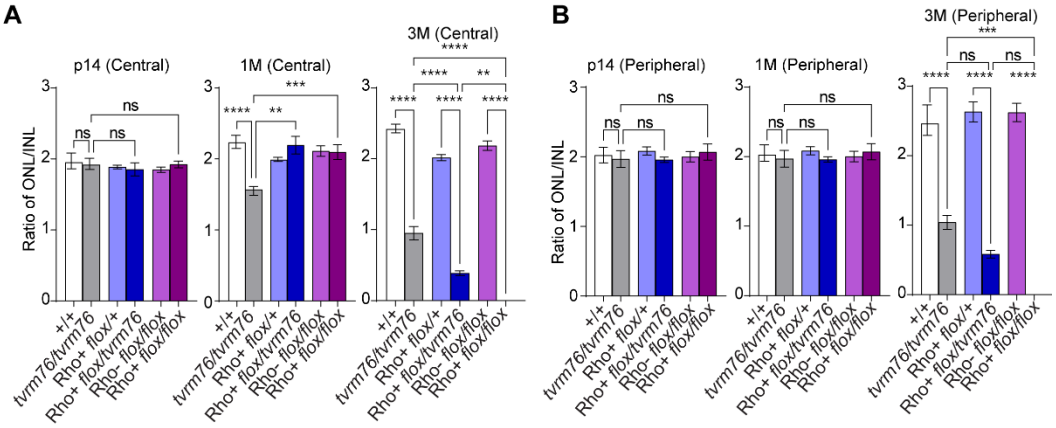

Supplementary 1. Photoreceptor degeneration in *tvrm76*. (A,B). Quantification of ONL nuclei degeneration relative to INL in the central and peripheral retinal regions. Significant loss of photoreceptors in *tvrm76* mice compared to their wild-type littermates and *Dpagt1* rod photoreceptor knockouts at one month of age in the central retina, while peripheral loss becomes significant at 3 months. Values represent mean ±SEM; n=3-6 **p<0.01;***p<0.001;****p<0.0001 (One-way ANOVA).

Preprints (www.preprints.org) | NOT PEER-REVIEWED | Posted: 4 August 2022 doi:10.20944/preprints202208.0106.v1

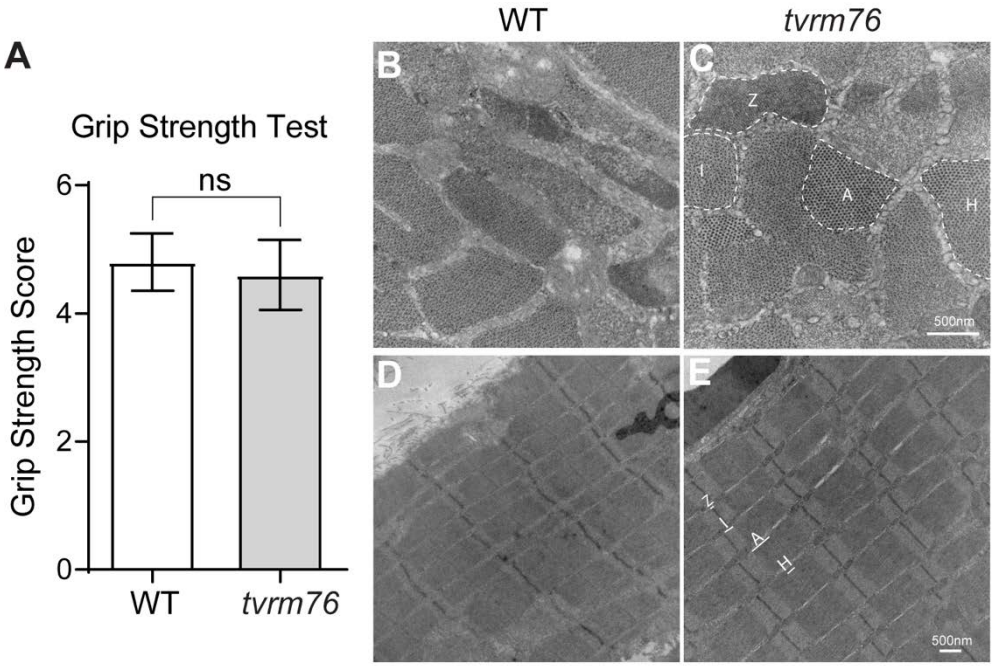

Scheme 2. Grip strength and muscular architecture in *tvrm76* and littermate WT controls. **(A)** No significant difference in grip strength of *tvrm76* compared to wildtype controls at 1 month of age. Values represent mean ±SEM; n=5 (p=0.999, Student t-test). **(B-E)** Transmission electron microscopy of gastrocnemius muscle samples in transverse **(B,C)** and longitudinal **(D,E)** sections. No presence of tubular aggregates or abnormal features were observed in *tvrm76* mutants compared to littermate controls at 2 months of age. Z=Z-line, I=I-Band, A=A-Band, H=H-Zone.

Appendix B.

Table 1. Primers for qPCR.

Gene	Sequences (5' – 3')
Actb	F: CCAGTTCGCCATGGATGACGATAT
	R: GTCAGGATACCTCTCTTGCTCTG
Atf4	F: TCGATGCTCTGTTTCGAATG
	R: AGAATGTAAAGGGGGCAACC
Hspa5	F: CCTCTCTGGTGATCAGGATA
	R: CGTGGAGAAGATCTGAGACT
Ddit3	F: CCACCACACCTGAAAGCAGAA
	R: AGGTGAAAGGCAGGGACTCA
Dpagt1	F: GGCCGGTCAGTCACTAGTCA
	R: GGTGTCTCCCACAAACACGC
Hsp90b1	F: GATGGTCTGGCAACATGGAG
	R: CGCCTTGGTGTCTGGTAGAA
Padi2	F: CAAGATCAAGCCCCACCTGAT
	R: AGTTGCCCCAACCAGTACTT

References

1. Chang, I.J.; He, M.; Lam, C.T. Congenital disorders of glycosylation. *Annals of translational medicine* **2018**, *6*.
2. Ondruskova, N.; Cechova, A.; Hansikova, H.; Honzik, T.; Jaeken, J. Congenital disorders of glycosylation: Still "hot" in 2020. *Biochim Biophys Acta Gen Subj* **2021**, *1865*, 129751.
3. Wilson, M.P.; Matthijs, G. The evolving genetic landscape of congenital disorders of glycosylation. *Biochim Biophys Acta Gen Subj* **2021**, *1865*, 129976.

 doi:10.20944/preprints202208.0106.v1

4. Jaeken, J.; Lefeber, D.; Matthijs, G. Clinical utility gene card for: DPAGT1 defective congenital disorder of glycosylation. *Eur J Hum Genet* **2015**, *23*.
5. Selcen, D.; Shen, X.M.; Brengman, J.; Li, Y.; Stans, A.A.; Wieben, E.; Engel, A.G. DPAGT1 myasthenia and myopathy: genetic, phenotypic, and expression studies. *Neurology* **2014**, *82*, 1822-1830.
6. Ng, B.G.; Freeze, H.H. Perspectives on glycosylation and its congenital disorders. *Trends in Genetics* **2018**, *34*, 466-476.
7. Dong, Y.Y.; Wang, H.; Pike, A.C.W.; Cochrane, S.A.; Hamedzadeh, S.; Wyszynski, F.J.; Bushell, S.R.; Royer, S.F.; Widdick, D.A.; Sajid, A., et al. Structures of DPAGT1 Explain Glycosylation Disease Mechanisms and Advance TB Antibiotic Design. *Cell* **2018**, *175*, 1045-1058 e1016.
8. Paprocka, J.; Jezela-Stanek, A.; Tylki-Szymanska, A.; Grunewald, S. Congenital Disorders of Glycosylation from a Neurological Perspective. *Brain Sci* **2021**, *11*.
9. Belaya, K.; Finlayson, S.; Slater, C.R.; Cossins, J.; Liu, W.W.; Maxwell, S.; McGowan, S.J.; Maslau, S.; Twigg, S.R.; Walls, T.J., et al. Mutations in DPAGT1 cause a limb-girdle congenital myasthenic syndrome with tubular aggregates. *Am J Hum Genet* **2012**, *91*, 193-201.
10. Belaya, K.; Finlayson, S.; Cossins, J.; Liu, W.W.; Maxwell, S.; Palace, J.; Beeson, D. Identification of DPAGT1 as a new gene in which mutations cause a congenital myasthenic syndrome. *Ann N Y Acad Sci* **2012**, *1275*, 29-35.
11. Yuste-Checa, P.; Vega, A.I.; Martin-Higueras, C.; Medrano, C.; Gamez, A.; Desviat, L.R.; Ugarte, M.; Perez-Cerda, C.; Perez, B. DPAGT1-CDG: Functional analysis of disease-causing pathogenic mutations and role of endoplasmic reticulum stress. *PLoS One* **2017**, *12*, e0179456.
12. Messenger, W.B.; Yang, P.; Pennesi, M.E. Ophthalmic findings in an infant with phosphomannomutase deficiency. *Doc Ophthalmol* **2014**, *128*, 149-153.
13. Thompson, D.A.; Lyons, R.J.; Russell-Eggitt, I.; Liasis, A.; Jagle, H.; Grunewald, S. Retinal characteristics of the congenital disorder of glycosylation PMM2-CDG. *J Inherit Metab Dis* **2013**, *36*, 1039-1047.
14. Heifetz, A.; Keenan, R.W.; Elbein, A.D. Mechanism of action of tunicamycin on the UDP-GlcNAc: dolichyl-phosphate GlcNAc-1-phosphate transferase. *Biochemistry* **1979**, *18*, 2186-2192.
15. Fliesler, S.J.; Basinger, S.F. Tunicamycin blocks the incorporation of opsin into retinal rod outer segment membranes. *Proceedings of the National Academy of Sciences* **1985**, *82*, 1116-1120.
16. Fliesler, S.J.; Rapp, L.M.; Hollyfield, J.G. Photoreceptor-specific degeneration caused by tunicamycin. *Nature* **1984**, *311*, 575-577.
17. Marek, K.W.; Vijay, I.K.; Marth, J.D. A recessive deletion in the GlcNAc-1-phosphotransferase gene results in peri-implantation embryonic lethality. *Glycobiology* **1999**, *9*, 1263-1271.
18. Krebs, M.P.; Collin, G.B.; Hicks, W.L.; Yu, M.; Charette, J.R.; Shi, L.Y.; Wang, J.; Naggert, J.K.; Peachey, N.S.; Nishina, P.M. Mouse models of human ocular disease for translational research. *PLoS One* **2017**, *12*, e0183837.
19. Won, J.; Shi, L.Y.; Hicks, W.; Wang, J.; Hurd, R.; Naggert, J.K.; Chang, B.; Nishina, P.M. Mouse model resources for vision research. *J Ophthalmol* **2011**, *2011*, 391384.
20. Li, S.; Chen, D.; Sauve, Y.; McCandless, J.; Chen, Y.J.; Chen, C.K. Rhodopsin-iCre transgenic mouse line for Cre-mediated rod-specific gene targeting. *Genesis* **2005**, *41*, 73-80.
21. Won, J.; Gifford, E.; Smith, R.S.; Yi, H.; Ferreira, P.A.; Hicks, W.L.; Li, T.; Naggert, J.K.; Nishina, P.M. RPGRIP1 is essential for normal rod photoreceptor outer segment elaboration and morphogenesis. *Hum Mol Genet* **2009**, *18*, 4329-4339.
22. Chang, B.; Hawes, N.L.; Hurd, R.E.; Davisson, M.T.; Nusinowitz, S.; Heckenlively, J.R. Retinal degeneration mutants in the mouse. *Vision Res* **2002**, *42*, 517-525.
23. Salom, D.; Jin, H.; Gerken, T.A.; Yu, C.; Huang, L.; Palczewski, K. Human red and green cone opsins are O-glycosylated at an N-terminal Ser/Thr–rich domain conserved in vertebrates. *Journal of Biological Chemistry* **2019**, *294*, 8123-8133.

24. Murray, A.R.; Vuong, L.; Brobst, D.; Fliesler, S.J.; Peachey, N.S.; Gorbatyuk, M.S.; Naash, M.I.; Al-Ubaidi, M.R. Glycosylation of rhodopsin is necessary for its stability and incorporation into photoreceptor outer segment discs. *Human molecular genetics* **2015**, *24*, 2709-2723.
25. Berson, E.L.; Rosner, B.; Weigel-DiFranco, C.; Dryja, T.P.; Sandberg, M.A. Disease progression in patients with dominant retinitis pigmentosa and rhodopsin mutations. *Investigative ophthalmology & visual science* **2002**, *43*, 3027-3036.
26. Nashine, S.; Bhootada, Y.; Lewin, A.S.; Gorbatyuk, M. Ablation of C/EBP homologous protein does not protect T17M RHO mice from retinal degeneration. *PLoS One* **2013**, *8*, e63205.
27. Michele, D.E.; Barresi, R.; Kanagawa, M.; Saito, F.; Cohn, R.D.; Satz, J.S.; Dollar, J.; Nishino, I.; Kelley, R.I.; Somer, H. Post-translational disruption of dystroglycan–ligand interactions in congenital muscular dystrophies. *Nature* **2002**, *418*, 417-421.
28. Van Den Boogert, M.A.; Larsen, L.E.; Ali, L.; Kuil, S.D.; Chong, P.L.; Loregger, A.; Kroon, J.; Schnitzler, J.G.; Schimmel, A.W.; Peter, J. N-glycosylation defects in humans lower low-density lipoprotein cholesterol through increased low-density lipoprotein receptor expression. *Circulation* **2019**, *140*, 280-292.
29. Tabas, I.; Ron, D. Integrating the mechanisms of apoptosis induced by endoplasmic reticulum stress. *Nature cell biology* **2011**, *13*, 184-190.
30. Wang, Q.; Wang, H.; Jia, Y.; Pan, H.; Ding, H. Luteolin induces apoptosis by ROS/ER stress and mitochondrial dysfunction in gliomablastoma. *Cancer chemotherapy and pharmacology* **2017**, *79*, 1031-1041.
31. Hu, H.; Tian, M.; Ding, C.; Yu, S. The C/EBP homologous protein (CHOP) transcription factor functions in endoplasmic reticulum stress-induced apoptosis and microbial infection. *Frontiers in immunology* **2019**, 3083.
32. Li, H.; You, L.; Tian, Y.; Guo, J.; Fang, X.; Zhou, C.; Shi, L.; Su, Y.Q. DPAGT1 ‐ Mediated Protein N ‐ Glycosylation Is Indispensable for Oocyte and Follicle Development in Mice. *Advanced Science* **2020**, *7*, 2000531.
33. Lehle, L.; Strahl, S.; Tanner, W. Protein glycosylation, conserved from yeast to man: a model organism helps elucidate congenital human diseases. *Angewandte Chemie International Edition* **2006**, *45*, 6802-6818.
34. Nicole, S.; Azuma, Y.; Bauche, S.; Eymard, B.; Lochmuller, H.; Slater, C. Congenital Myasthenic Syndromes or Inherited Disorders of Neuromuscular Transmission: Recent Discoveries and Open Questions. *J Neuromuscul Dis* **2017**, *4*, 269-284.
35. Engel, A.G.; Shen, X.M.; Selcen, D.; Sine, S.M. Congenital myasthenic syndromes: pathogenesis, diagnosis, and treatment. *Lancet Neurol* **2015**, *14*, 420-434.
36. Ng, B.G.; Underhill, H.R.; Palm, L.; Bengtson, P.; Rozet, J.M.; Gerber, S.; Munnich, A.; Zanlonghi, X.; Stevens, C.A.; Kircher, M., et al. DPAGT1 Deficiency with Encephalopathy (DPAGT1-CDG): Clinical and Genetic Description of 11 New Patients. *JIMD Rep* **2019**, *44*, 85-92.
37. Engel, A.G. Genetic basis and phenotypic features of congenital myasthenic syndromes. *Handbook of Clinical Neurology* **2018**, *148*, 565-589.
38. Issop, Y.; Hathazi, D.; Khan, M.M.; Rudolf, R.; Weis, J.; Spendiff, S.; Slater, C.R.; Roos, A.; Lochmüller, H. GFPT1 deficiency in muscle leads to myasthenia and myopathy in mice. *Human molecular genetics* **2018**, *27*, 3218-3232.
39. Gidaro, T.; Vandenbrande, L.; Malfatti, E.; Labasse, C.; Carlier, P.; Romero, N.; Servais, L.; Böhm, J. Congenital Myasthenic Syndromes and Myasthenia: P. 70 New homozygous mutation in DPAGT1 gene leading to LG-CMS with tubular aggregates. *Neuromuscular Disorders* **2018**, *28*, S51.
40. Nicolau, S.; Kao, J.C.; Liewluck, T. Trouble at the junction: when myopathy and myasthenia overlap. *Muscle & Nerve* **2019**, *60*, 648-657.
41. Bogdanova-Mihaylova, P.; Murphy, R.; Alexander, M.; McHugh, J.; Foley, A.R.; Brett, F.; Murphy, S. Congenital myasthenic syndrome due to DPAGT1 mutations mimicking congenital myopathy in an Irish family. *European Journal of Neurology* **2018**, *25*, e22-e23.

42. Kanaki, N.; Matsuda, A.; Dejima, K.; Murata, D.; Nomura, K.H.; Ohkura, T.; Gengyo-Ando, K.; Yoshina, S.; Mitani, S.; Nomura, K. UDP-N-acetylglucosamine-dolichyl-phosphate N-acetylglucosaminephosphotransferase is indispensable for oogenesis, oocyte-to-embryo transition, and larval development of the nematode Caenorhabditis elegans. *Glycobiology* **2019**, *29*, 163-178.
43. Finlayson, S.; Palace, J.; Belaya, K.; Walls, T.J.; Norwood, F.; Burke, G.; Holton, J.L.; Pascual-Pascual, S.I.; Cossins, J.; Beeson, D. Clinical features of congenital myasthenic syndrome due to mutations in DPAGT1. *J Neurol Neurosurg Psychiatry* **2013**, *84*, 1119-1125.
44. Basiri, K.; Belaya, K.; Liu, W.W.; Maxwell, S.; Sedghi, M.; Beeson, D. Clinical features in a large Iranian family with a limb-girdle congenital myasthenic syndrome due to a mutation in DPAGT1. *Neuromuscul Disord* **2013**, *23*, 469-472.
45. Estephan, E.P.; Zambon, A.A.; Thompson, R.; Polavarapu, K.; Jomaa, D.; Töpf, A.; Helito, P.V.; Heise, C.O.; Moreno, C.A.; Silva, A.M. Congenital myasthenic syndrome: Correlation between clinical features and molecular diagnosis. *European journal of neurology* **2022**, *29*, 833-842.
46. Citro, V.; Cimmaruta, C.; Monticelli, M.; Riccio, G.; Hay Mele, B.; Cubellis, M.V.; Andreotti, G. The analysis of variants in the general population reveals that PMM2 is extremely tolerant to missense mutations and that diagnosis of PMM2-CDG can benefit from the identification of modifiers. *International journal of molecular sciences* **2018**, *19*, 2218.
47. Schjoldager, K.T.; Narimatsu, Y.; Joshi, H.J.; Clausen, H. Global view of human protein glycosylation pathways and functions. *Nature reviews Molecular cell biology* **2020**, *21*, 729-749.
48. Eichler, J. Protein glycosylation. *Current Biology* **2019**, *29*, R229-R231.
49. Van Landuyt, L.; Lonigro, C.; Meuris, L.; Callewaert, N. Customized protein glycosylation to improve biopharmaceutical function and targeting. *Current opinion in biotechnology* **2019**, *60*, 17-28.
50. Esmail, S.; Manolson, M.F. Advances in understanding N-glycosylation structure, function, and regulation in health and disease. *European Journal of Cell Biology* **2021**, *100*, 151186.
51. Qi, Z.; Chen, L. Endoplasmic reticulum stress and autophagy. *Autophagy: Biology and Diseases* **2019**, 167-177.
52. Choy, K.W.; Murugan, D.; Mustafa, M.R. Natural products targeting ER stress pathway for the treatment of cardiovascular diseases. *Pharmacological Research* **2018**, *132*, 119-129.
53. Medinas, D.B.; Rozas, P.; Traub, F.M.; Woehlbier, U.; Brown, R.H.; Bosco, D.A.; Hetz, C. Endoplasmic reticulum stress leads to accumulation of wild-type SOD1 aggregates associated with sporadic amyotrophic lateral sclerosis. *Proceedings of the National Academy of Sciences* **2018**, *115*, 8209-8214.
54. Lebedeva, I.V.; Wagner, M.V.; Sahdeo, S.; Lu, Y.F.; Anyanwu-Ofili, A.; Harms, M.B.; Wadia, J.S.; Rajagopal, G.; Boland, M.J.; Goldstein, D.B. Precision genetic cellular models identify therapies protective against ER stress. *Cell Death Dis* **2021**, *12*, 770.
55. Fairfield, H.; Gilbert, G.J.; Barter, M.; Corrigan, R.R.; Curtain, M.; Ding, Y.; D'Ascenzo, M.; Gerhardt, D.J.; He, C.; Huang, W., et al. Mutation discovery in mice by whole exome sequencing. *Genome Biol* **2011**, *12*, R86.
56. Hawes, N.L.; Chang, B.; Hageman, G.S.; Nusinowitz, S.; Nishina, P.M.; Schneider, B.S.; Smith, R.S.; Roderick, T.H.; Davisson, M.T.; Heckenlively, J.R. Retinal degeneration 6 (rd6): a new mouse model for human retinitis punctata albescens. *Invest Ophthalmol Vis Sci* **2000**, *41*, 3149-3157.
57. Krebs, M.P.; Xiao, M.; Sheppard, K.; Hicks, W.; Nishina, P.M. Bright-Field Imaging and Optical Coherence Tomography of the Mouse Posterior Eye. *Methods Mol Biol* **2016**, *1438*, 395-415.
58. Kong, Y.; Zhao, L.; Charette, J.R.; Hicks, W.L.; Stone, L.; Nishina, P.M.; Naggert, J.K. An FRMD4B variant suppresses dysplastic photoreceptor lesions in models of enhanced S-cone syndrome and of Nrl deficiency. *Hum Mol Genet* **2018**, *27*, 3340-3352.
59. Burgess, R.W.; Cox, G.A.; Seburn, K.L. Neuromuscular disease models and analysis. *Methods Mol Biol* **2010**, *602*, 347-393.

60. Motley, W.W.; Seburn, K.L.; Nawaz, M.H.; Miers, K.E.; Cheng, J.; Antonellis, A.; Green, E.D.; Talbot, K.; Yang, X.L.; Fischbeck, K.H., et al. Charcot-Marie-Tooth-linked mutant GARS is toxic to peripheral neurons independent of wild-type GARS levels. *PLoS Genet* **2011**, *7*, e1002399.

61. Schindelin, J.; Arganda-Carreras, I.; Frise, E.; Kaynig, V.; Longair, M.; Pietzsch, T.; Preibisch, S.; Rueden, C.; Saalfeld, S.; Schmid, B., et al. Fiji: an open-source platform for biological-image analysis. *Nat Methods* **2012**, *9*, 676-682.

62. Ramachandra Rao, S.; Skelton, L.A.; Wu, F.; Onysk, A.; Spolnik, G.; Danikiewicz, W.; Butler, M.C.; Stacks, D.A.; Surmacz, L.; Mu, X., et al. Retinal Degeneration Caused by Rod-Specific Dhdds Ablation Occurs without Concomitant Inhibition of Protein N-Glycosylation. *iScience* **2020**, *23*, 101198.

63. Murray, A.R.; Vuong, L.; Brobst, D.; Fliesler, S.J.; Peachey, N.S.; Gorbatyuk, M.S.; Naash, M.I.; Al-Ubaidi, M.R. Glycosylation of rhodopsin is necessary for its stability and incorporation into photoreceptor outer segment discs. *Hum Mol Genet* **2015**, *24*, 2709-2723.